*Astronomy & Astrophysics* manuscript no. ART˙A2163B2 May 22, 2019
(DOI: will be inserted by hand later)



# The cluster of galaxies A 2163B at z ∼ 0.2

## II – Colour gradients, $r_e$–$<\mu>_e$ relations, and the Photometric Plane. ⋆

F. La Barbera[1], G. Busarello[1], P. Merluzzi[1], M. Massarotti[1], A. Mercurio[2], and M. Capaccioli[1]

[1] I.N.A.F., Istituto Nazionale di Astrofisica Osservatorio Astronomico di Capodimonte, Via Moiariello 16, I-80131 Napoli
email: labarber@na.astro.it

[2] Università degli Studi di Trieste, Department of Astronomy, Trieste

Received ; accepted

**Abstract.** We present the structural parameters (half light radius $r_e$, mean surface brightness $<\mu>_e$ within $r_e$ and Sersic index n) in the R, I and K bands for N ∼ 60 galaxies in the cluster A 2163B at z ∼ 0.2. The structural parameters are used to estimate the internal colour gradients of bulge–dominated (n > 2) galaxies. For the first time, we perform a comparative optical/NIR analysis of the $\log r_e$–$<\mu>_e$ relation, also known as Kormendy relation (KR), and derive the so-called Photometric Plane in the K band. Colour gradients are negligible at optical wavelengths, while are significantly negative in the optical-NIR, amounting on average to −0.48 ± 0.06. This result is in agreement with our previous measurements of colour gradients at intermediate redshifts, implying the presence of a metallicity gradient in galaxies of about −0.2 dex per radial decade. We derive unbiased estimates of the slope and of the zeropoint of the $\log r_e$–$<\mu>_e$ relation in the R and K bands, respectively, and analyze the waveband dependence of these quantities by taking into account the role of the CM relation and of the colour gradients. We find that the optical–NIR variation of the KR slope implies that colour gradients do not vary with galaxy size or become less steep for galaxies of larger size. This result is in sharp contrast with what would be expected in the monolithic collapse scenario, while can be well understood in a hierarchical merging framework. Finally, we derive the NIR Photometric Plane (PHP) at z ∼ 0.2, attempting to correct both for the correlations between the uncertainties on the structural parameters and for the selection effects of the samples. We find that the PHP coefficients are consistent with those of the local relation and that its observed dispersion is similar to that of the 'spectroscopic' Fundamental Plane (FP), as discussed by Graham (2002). However, the

intrinsic scatter around the Photometric Plane could be significantly larger with respect to that of the FP, although smaller with respect to that of the KR.

**Key words.** Galaxies: clusters: individual: A 2163B – Galaxies: photometry – Galaxies: fundamental parameters

## 1. Introduction

The study of the structural properties of galaxies at different redshifts provides a wealth of information by which galaxy formation and evolution can be investigated, both trough the correlations between the quantities that characterize the internal light distribution of galaxies and trough the analysis of the waveband dependence of such quantities.

The multi-waveband analysis informs on the internal colour gradients (CGRs) of galaxies, and therefore on the radial gradients of the properties of their stellar populations (SPs), such as age, metallicity and dust content. Nearby galaxies have on average negative CGRs, their SPs becoming bluer toward the periphery (Peletier et al., 1990; Peletier, Valentijn, and Jameson, 1990). Due to the little evolution of colour gradients over redshift, metallicity seems to be the primary driver of the SP gradients for spheroidal galaxies, as demonstrated both by optical studies (e.g. Saglia et al. 2000; Tamura and Ohta 2000) and by optical–NIR CGR measurements (La Barbera et al., 2002, 2003a, hereafter LBM02 and LBM03a, respectively). The age gradients, however, are not fully ruled out by the present data (Saglia et al. 2000, LBM03a), while the effects of dust absorption remain still substantially unresolved. The presence of metallicity gradients can be well explained in the monolithic formation scenario of early-type galaxies (Larson, 1974), due to the later beginning of the galactic wind in the inner galaxy regions. However, it can also be accommodated within the hierarchical merging framework, since metallicity gradients are settled in disk galaxies at high redshift, and more massive early-types form on average from the merging of larger disks (Kauffmann, 1996). The present data do not allow to discriminate between the two formation scenarios, although some interesting clues come from the study of colour gradients of disk galaxies at different redshifts (see LBM03a).

Structural parameters, such as the effective (half–light) radius $r_e$, the mean surface brightness $<\mu>_e$ within $r_e$ and the Sersic index n, are correlated by various relations, whose physical origins reside both on the properties of the SPs of galaxies and on the dynamical structure of these systems. For the population of early–type galaxies, one of the most interesting correlation is that between $\log r_e$ and $<\mu>_e$, also known as Kormendy relation (KR). As shown by Capaccioli, Caon, and D'Onofrio (1992), early-type galaxies and bulges form two distinct families in the plane of the effective parameters: that of the bright early-types, following the KR, and another 'ordinary' family, whose properties are more disperse and heterogeneous. Recently, Graham and Guzmàn (2003) showed that there is no real dichotomy between the two fami-

*Send offprint requests to*: F. La Barbera

⋆ Based on observations collected at European Southern Observatory (ESO 65.O-0251, 69.D-0653).

lies, but their observed properties are well explained by a systematic change in the profile shape with galaxy luminosity. The evolution of the zeropoint of the KR has been largely investigated at optical wavebands in order to constrain the major formation epoch of galaxy SPs and to perform the Tolman test for the cosmological expansion (Sandage and Perelmuter, 1991; Pahre, Djorgovski, and de Carvalho, 1996; Sandage and Lubin, 2001; Lubin and Sandage, 2001; Barger et al., 1998; Ziegler et al., 1999). On the other hand, the slope of the KR is an interesting tool to gain insight into the properties of the galaxy SPs as a function of galaxy size (Ziegler et al. 1999, La Barbera et al. 2003b, hereafter LBM03b), which is a crucial prediction of hierarchical merging scenarios.

As recently shown by Graham (2002, hereafter GRA02), early-type galaxies also follow a three-dimensional relation between $\log r_e$, $<\mu>_e$ and $\log n$, whose expression is similar to that of the 'spectroscopic' Fundamental Plane (FP), once that velocity dispersions are replaced by Sersic indices. This 'photometric plane' (hereafter PHP) has an observed scatter which could be similar to that of the Fundamental Plane (FP) relation, and carries interesting information on the physical properties of galaxies and their origin. The existence of a three-dimensional plane in the space of structural parameters has been explained by the fact that the specific entropy of elliptical galaxies is not constant (Lima Neto, Gerbal, & Márquez, 1999), but it is an increasing function of galaxy luminosity (Márquez et al., 2000).

In the present study, we analyze the structural properties of the population of A 2163B, a cluster of galaxies close to the Abell cluster A 2163. As shown in La Barbera et al. (2003c, paper I), A 2163B is a cluster of galaxies at $z \sim 0.2$, likely involved in a merging event with A 2163. All the photometric properties of galaxies in the field of A 2163B, including BVRIK magnitudes and colours, and RIK structural parameters, are given in Tab. 2 of paper I. The layout of the paper is as follows. In Sec. 1 we describe the samples used for the present analysis. The derivation of structural parameters is outlined in Sec. 2. Sec. 3 deals with the comparison of structural parameters and with the analysis of the internal colour gradients of galaxies. The correlations between the structural parameters are discussed in Secs. 4 and 5: in Sec. 4, we perform an optical/NIR comparative study of the $\log r_e$–$<\mu>_e$ relation, while in Sec. 5 we use the K-band data to analyze the PHP for the population of spheroids in A 2163B. Discussion and conclusions follow in Sec. 6.

In the following we assume the cosmology $H_0 = 70$ Km s$^{-1}$Mpc$^{-1}$, $\Omega_m = 0.3$ and $\Omega_\Lambda = 0.7$. With these parameters the age of the universe is $\sim 13.5$ Gyr, and the redshift $z = 0.2$ corresponds to a lookback time of $\sim 2.5$ Gyr.

## 2. The samples

The galaxies used for the present analysis belong to the cluster A 2163B at redshift $z \sim 0.2$. The cluster membership was derived as detailed in paper I, by using BVRIK photometry to obtain photometric redshifts. Structural parameters were derived in the R and I bands for all

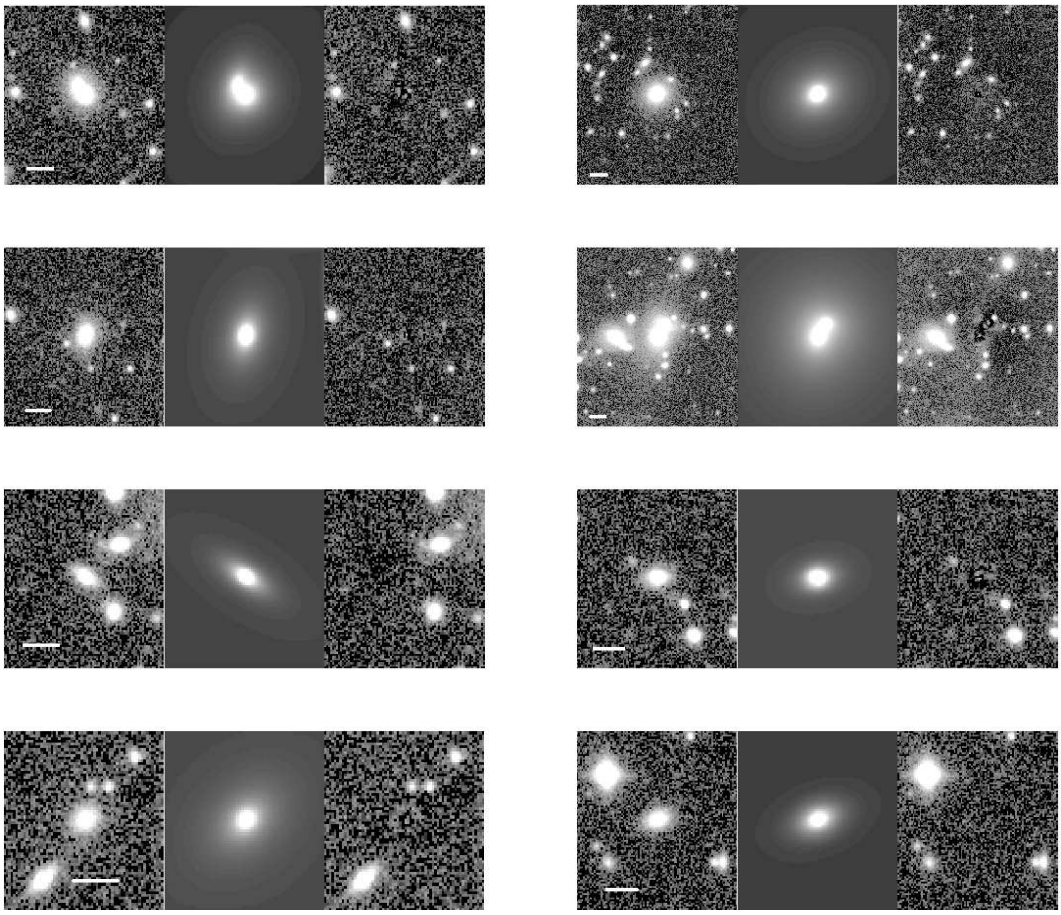

**Fig. 1.** 2D fits of galaxies in the K-band image. For each plot, from left to right, the galaxy image, the 2D model and the residual map are shown. The size of the horizontal white bar is 5“.

galaxies brighter than $R_T = 19.5$, and in the K band for galaxies brighter than $K_T = 16.5$. These selection criteria were chosen in order to obtain reliable structural parameters from the A 2163B photometry, and result from numerical simulations performed as described in LBM02. A further selection was performed a posteriori by excluding few faint galaxies in the I and K bands because of the strong contamination from close objects, and/or of the poor two-dimensional fits. The resulting samples include N = 64, 62 and 58 galaxies for the R, I and K bands, respectively, with N = 62 objects in common between the R and I bands, and N = 58 galaxies in common between the R and K bands.

## 3. Surface photometry

Surface photometry was derived by fitting galaxy images with 2D models convolved with the PSF, as detailed in LBM02. As shown in that paper, the 2D approach allows reliable structural parameters to be obtained for galaxies at intermediate redshifts ($z \sim 0.3$) from ground based data taken under ordinary observing conditions (seeing FWHM $\sim 1.0''$ and pixel scale $\sim 0.3''$/pxl). Galaxy models were parametrized by the Sersic law:

$$I(r) = I_0 \cdot \exp(-b \cdot (r/r_e)^{1/n}), \quad (1)$$

where r is the equivalent radius, $r_e$ is the effective (half-light) radius, $I_0$ is the central surface brightness, n is the Sersic index, and b is a constant ($b \sim 2n - 1/3$, see Caon, Capaccioli, and D'Onofrio 1993). For each galaxy, nearby objects were masked interactively, while overlapping galaxies were fitted simultaneously. The chi–square minimization was performed by the Levenberg-Marquardt method, deriving a total of six best-fit parameters: the center coordinates, the effective radius, the central surface brightness, the position angle PA and the axis ratio b/a. The mean surface brightness within $r_e$, $<\mu>_e$, and the total magnitude $m_T$ were computed from the fitting parameters by using the well known properties of the Sersic law. The typical uncertainties on galaxy parameters were estimated by comparing structural parameters between different wavebands (see next section). The PSF models were obtained by a multi-gaussian expansion of the images of bright unsaturated stars in the cluster field. For the R and I bands, all the stars were fitted simultaneously, resulting in a single PSF model. For the K band, the PSF turned out to vary across the field, showing significant deviations from the circular shape in the North-East corner of the frame. Since star images were available at different positions across the field, with an almost uniform coverage, we adopted for each galaxy the PSF model obtained from the closest star. PSF distortions were treated by adopting gaussian functions with elliptical isophotes (see LBM03a). Fig. 1 plots, as an example, the K-band 2D fitting of some galaxies in the cluster field. The models turned out to give a very good description of the galaxy images.

## 4. Optical–NIR internal structure of cluster galaxies

We analyze the internal optical–NIR structure of galaxies in A 2163B by (1) a straight comparison of structural parameters (Sec. 4.1) and (2) estimating the internal colour gradients of galaxies (Sec. 4.2). This subject was also investigated in LBM03a, who first attempted to analyze the evolution of the UV–NIR structural properties of both the populations of disk ($n < 2$) dominated and spheroidal ($n > 2$) galaxies down to redshift $z \sim 0.6$, by using a large sample of cluster galaxies (N = 270). Since the number of disks in common between the R and K bands turns out to be negligible (N = 5 out of 58), we did not attempt[1] to study the dependence of the structural properties on the shape of the light profile. The following results will refer, therefore, to the spheroidal population of A 2163B.

### *4.1. Comparison of structural parameters*

Fig. 2 shows the comparison of structural parameters for the N = 62 galaxies in common between the R- and I-bands. Differences are always computed between the shorter and the longer wavelength. The following quantities are considered: effective radii and mean surface brightnesses, Sersic indices, and the combination of $r_e$ and $<\mu>_e$ which enters the Fundamental Plane:

[1] Disk galaxies are included in the analysis of Sec. 4.1 and 4.2. However, the results remain unchanged after excluding these galaxies from the samples.

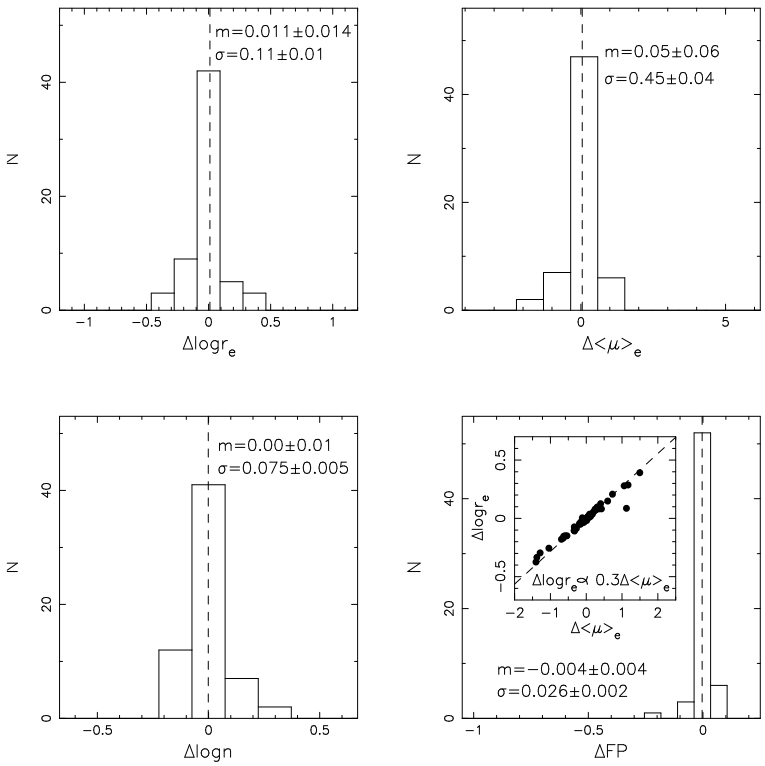


**Fig. 2.** Comparison of structural parameter in the optical. For each panel, differences are computed between R and I bands. The correlation between effective parameters is shown inside the lower right panel.

FP = $\log r_e - 0.3 \cdot <\mu>_e$. The differences in $<\mu>_e$ were corrected by subtracting the R – I colour for each galaxy. The mean value, m, and the standard deviation, $\sigma$, of each distribution are shown in Fig. 2, while in the lower right panel we also plot the correlation between $\Delta \log r_e$ and $\Delta <\mu>_e$. Optical parameters are in remarkable agreement, with mean differences that are fully consistent with zero for each quantity. This is consistent with previous studies, who found very small variation in the optical–optical properties of the light distribution for both nearby and intermediate redshift galaxies (e.g. Idiart et al. 2002; Tamura and Ohta 2000; Saglia et al. 2000). For this reason, we used the distributions of Fig. 2 to estimate the uncertainties on $\log r_e$, $<\mu>_e$ and $\log n$, by computing the covariance matrix of the differences between the R- and I-band parameters. The standard deviations of the distributions amount to $\sim 25\%$ in $r_e$, $\sim 0.45$ mag/arcsec$^2$ in $<\mu>_e$ and $\sim 18\%$ in n. We note, however, that due to the well known tight correlation between the uncertainties on the effective parameters (see e.g. Jørgensen, Franx, and Kjærgaard 1995), the FP term has a much smaller dispersion: only 6%.

Differences between R- and K-band structural parameters are shown in Fig. 3, where the mean surface brightnesses were corrected by using the R – K galaxy colours. The mean values of the distributions show that cluster galaxies are more concentrated in the NIR than in the optical, having NIR effective radii which are on average $\sim 40\%$ smaller than in the R-band ($\overline{\Delta \log r_e} = +0.16$), and Sersic indices slightly larger in the K-band (although the last difference is

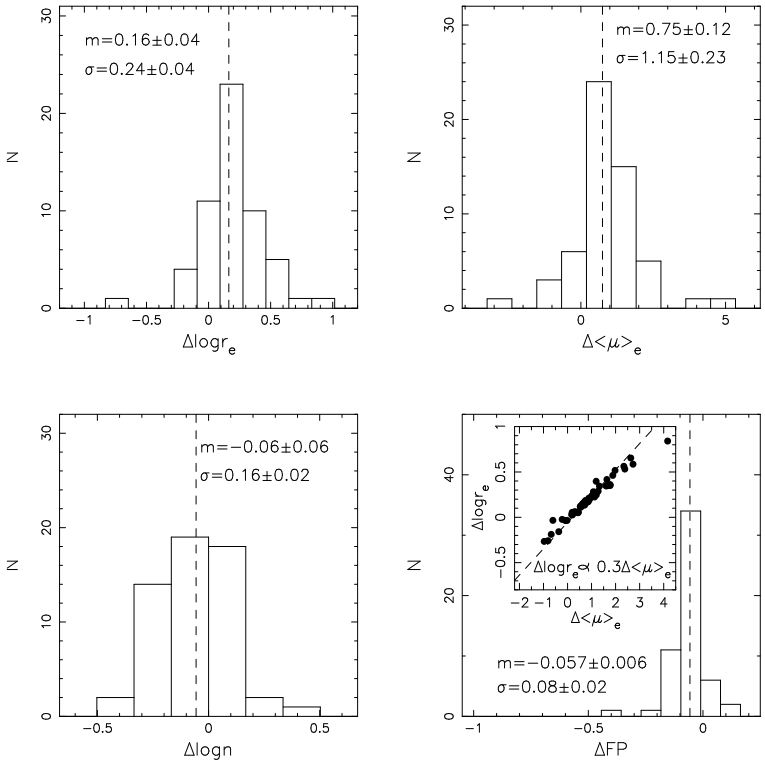


**Fig. 3.** Same of Fig. 2 for the R- and K-band parameters.

not statistically significant). The mean difference of $\Delta<\mu>_e$ can be fully explained by using the definition of total magnitude $m_T = -2.5\log(2\pi) - 5\log r_e + <\mu>_e$, and computing the difference between R- and K-band total magnitudes:

$$R_T - K_T = -5\Delta\log r_e + <\mu>_e^R - <\mu>_e^K. \quad (2)$$

From $\Delta<\mu>_e \simeq <\mu>_e^R - <\mu>_e^K - (R_T - K_T)$, it follows that $\Delta<\mu>_e = 5\Delta\log r_e$, which, for $\overline{\Delta\log r_e} = +0.16$, gives $\overline{\Delta<\mu>_e} \sim 0.8$, in agreement with the mean value reported in Fig. 3. The same procedure allows the mean difference of the FP variable to be explained.

The dispersion of the distributions in Fig. 3 is due (1) to the uncertainties on both the R- and K-band parameters, and (2) to the intrinsic scatter of the optical–NIR properties of galaxies. We verified by numerical simulations (performed as described in LBM02) that the uncertainties on the K-band structural parameters are as large as or smaller than those estimated for the optical wavebands. This implies that the dispersions of the histograms in Fig. 3 have mainly an intrinsic origin. In Secs. 5 and 6, in order to describe the uncertainties on $\log r_e$, $<\mu>_e$ and $\log n$, we adopted the same covariance matrix for both the optical and the NIR data. By looking at Fig. 3, we stress again the small dispersion in the FP variable, that amounts to $\sim 0.08$ dex.

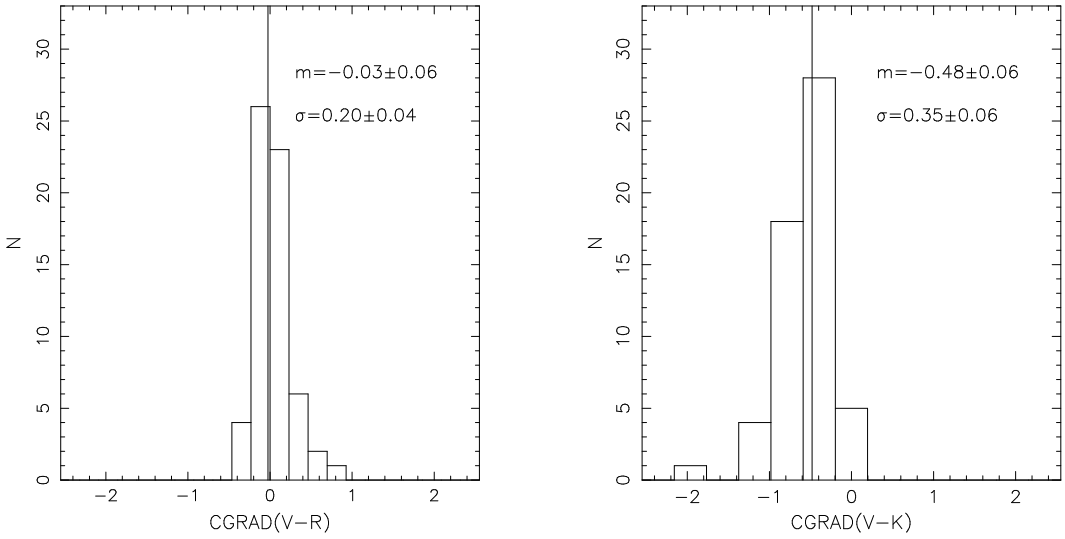


**Fig. 4.** Distributions of V − R and V − K colour gradients. The mean values are marked by a solid line.

### *4.2. Colour gradients*

For galaxies whose light profile is well described by the Sersic law, the internal colour gradient can be computed from the values of the effective radii and of the Sersic indices in the different wavebands, as described in LBM02 (see their Eq. 4).

The distributions of colour gradients for the galaxies of A 2163B are shown in Fig. 4, where we wrote the R−I and R−K colour gradients as V−R and V−K restframe gradients, respectively. By using different galaxy templates from the GISSEL00 code (Bruzual and Charlot, 1993), we verified, in fact, that the conversion from R − I (R − K) at z = 0.2 into V − R (V − K) at z = 0 is independent of the spectral type (for $z_f > 1$), with $1\sigma$ variations of 0.01 and 0.03 mag between different spectral models for the optical–optical and the optical–NIR colours, respectively. As expected on the basis of the structural parameters, galaxies show optical–optical colour gradients which are fully consistent with zero, while the V-K colour gradients are negative for most galaxies, implying that their SPs are on average redder in the center. The mean value of the optical–NIR gradient is −0.48, which implies that galaxies become ∼ 0.5 mag bluer per decade of radius toward the periphery. The value of grad(V − K) is consistent with the colour gradient estimate of LBM03a (about −0.4 mag/dex).

## 5. Optical–NIR Kormendy relations

The $\log r_e$–$<\mu>_e$ diagrams for the galaxies of A 2163B are shown in Fig. 5 for the R and K bands. The I band data are not considered since they do not add relevant information to the analysis. For each band, we excluded the disks (n < 2) and the galaxies for which the total magnitude, estimated by the structural parameters, is fainter than the completeness magnitude. This selection results in N = 52 and N = 53 galaxies in the R and K bands, respectively. For what concerns the NIR data, we also excluded two galaxies that have small radii and low surface brightness and for

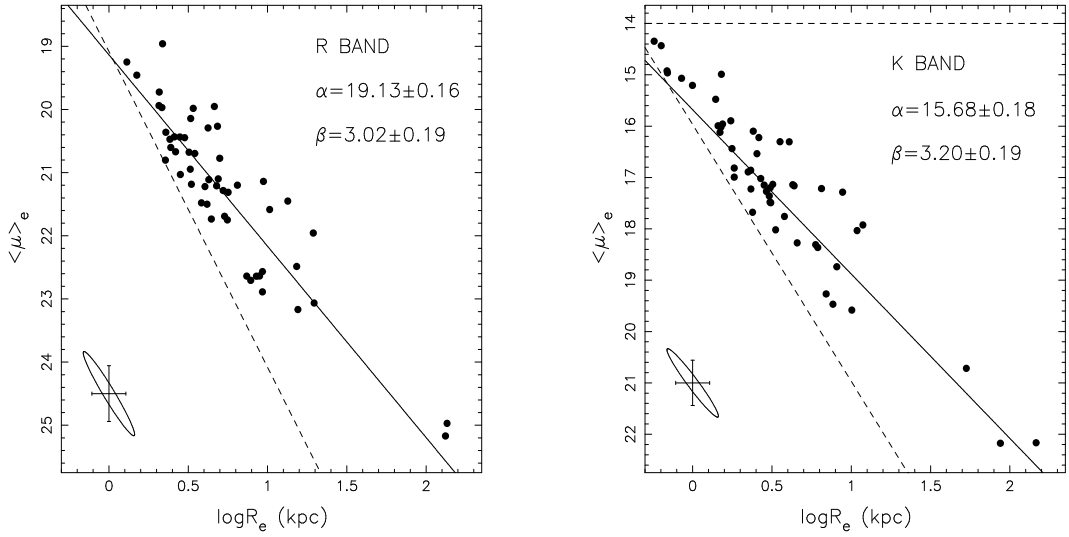


**Fig. 5.** Kormendy relations in R- and K-bands. Dashed lines mark the completeness magnitudes and the surface brightness cut (right panel) of each sample. The typical uncertainties on the effective parameters are indicated by the ellipses in the lower left corner of each panel. The ellipses mark the contours that enclose a probability of 68% for a 2D normal deviate.

which, therefore, structural parameters are possibly affected by a larger uncertainty. The K-band sample consists of N = 51 objects. In order to describe the $\log r_e$–$<\mu>_e$ sequence, we consider the following equation for each waveband M:

$$<\mu>_e^M = \alpha_M + \beta_M \cdot \log R_e^M \quad (3)$$

where $R_e$ is the effective radius in kpc, $\alpha_M$ and $\beta_M$ are the zeropoint and the slope of the relation. The evolution of the slope, of the zeropoint and of the intrinsic dispersion of the KR has been recently studied in the optical by LBM03b, who showed that these properties do not change significantly over redshift at least down to $z \sim 0.6$. They found $\beta = 2.92 \pm 0.08$, an intrinsic dispersion of $0.4 \pm 0.03$ mag/arcsec$^2$, and a KR zeropoint of $18.95 \pm 0.08$ mag/arcsec$^2$ in the R band at $z \sim 0.21$. In order to derive the values of $\alpha$ and $\beta$ for A 2163B, we applied the BMLS fitting procedure (see LBM03b), which allows the selection criteria to be taken into account, providing un-biased estimates of the KR coefficients. The fitting results are reported in Fig. 5. For what concerns the dispersion of the KRs, its value turns out to be consistent between the R and K bands, amounting to $0.65 \pm 0.12$ in $<\mu>_e$ and to $0.22 \pm 0.04$ in $\log r_e$. The R-band slope of the $\log r_e$–$<\mu>_e$ relation is fully consistent with that of LBM03b, in agreement with their finding that this coefficient does not evolve significantly over redshift. By adopting $\beta = 2.92$ in the fit, we obtain $\alpha_R = 19.16 \pm 0.10$ and, therefore, also the R-band zeropoint turns out to be in agreement with the result of LBM03b, once that measurement errors are taken into account. By subtracting in quadrature from the observed scatter around the KR the amount of dispersion due to the measurement uncertainties[2] on $\log r_e$ and $<\mu>_e$, we obtain the following estimate of the

[2] To this aim, we took into account the correlation of the uncertainties on $\log r_e$ and $<\mu>_e$.

intrinsic dispersion of the KR: $0.6 \pm 0.13$ mag/arcsec$^2$ ($0.21 \pm 0.04$ dex in $r_e$). This value is a little larger than (but consistent with) the estimate of LBM03b.

In order to compare the coefficients of the optical and NIR $\log r_e$–$<\mu>_e$ sequences, we have to take into account (1) the variation of the galaxy colour along the sequence due to the CM relation and (2) the waveband dependence of $r_e$ and $<\mu>_e$ due to internal colour gradients. By using Eq. 1 of paper I (that is the CM equation), and Eqs. 2 and 3, we obtain the following relation:

$$\begin{aligned} &<\mu>_e^K = <\mu>_e^R - 5 \cdot (\log R_e^R - \log R_e^K) - (R_T - K_T) = \\ &(1+\Delta)^{-1} \cdot \left[\alpha_R - \Gamma + 2.5 \cdot \Delta \cdot \log 2\pi - (5 - \beta_R) \cdot \log \frac{R_e^R}{R_e^K} + (\beta_R + 5\Delta) \cdot \log R_e^K\right] = \\ &\alpha'_K + \beta'_K \cdot \log R_e^K + \gamma'_K \cdot \left(\log \frac{R_e^R}{R_e^K} - \overline{\log \frac{R_e^R}{R_e^K}}\right), \end{aligned} \tag{4}$$

where $\Gamma$ and $\Delta$ are the zeropoint and the slope of the R – K vs. $K_T$ colour magnitude relation (see paper I), $\alpha'_K = (1+\Delta)^{-1} \cdot \left[\alpha_R - \Gamma + 2.5 \cdot \Delta \cdot \log 2\pi - (5 - \beta_R) \cdot \overline{\log(R_e^R/R_e^K)}\right]$, $\beta'_K = (1+\Delta)^{-1} \cdot (\beta_R + 5\Delta)$, and $\gamma'_K = -(5 - \beta_R) \cdot (1+\Delta)^{-1}$. We note that the value of $\alpha'_K$ corresponds to the zeropoint of the NIR KR, while $\beta'_K$ is equal to $\beta_K$ only if the third term of the last member of Eq. 4 vanishes, that is if the ratio of optical to NIR effective radii and, therefore, the internal colour gradients of galaxies do not vary systematically along the KR. By using the coefficients of the CM relation derived in Sec.4.1 of paper I, the mean ratio of optical to NIR effective radii ($\sim 0.16$), and the R-band KR coefficients ($\alpha = 19.16$ and $\beta = 2.92$), we obtain $\alpha'_K = 15.57$, $\beta'_K = 2.76$ and $\gamma'_K = -2.23$. The value of $\alpha'_K$ is in good agreement with that of $\alpha_K$, while the value of $\beta'_K$ is only marginally consistent with $\beta_K$, with a difference of $2.3\sigma$. Since the value of $\gamma'_K$ is negative, this difference could be explained if the $R_e^R/R_e^K$ ratio would become smaller for larger values of $R_e^K$, implying that larger galaxies have a less steep colour gradient. Fig. 6 plots $\log(R_e^R/R_e^K)$ and grad(R – K) as a function of $\log R_e^K$. Although the figure favors the trend suggested by the difference of $\beta'_K$ and $\beta_K$, the error bars do not allow such a trend to be definitively proven. We point out, however, that the previous results are in clear disagreement with a possible steepening of colour gradients with galaxy size, since it would make the discrepancy between $\beta_K$ and $\beta'_K$ strongly significant. This point will be further addressed in Sec. 7.

## 6. The NIR 'Photometric Plane'

Fig. 7 plots different projections of the distribution of galaxies in the space of the NIR structural parameters[3]. As shown in Fig 7a, effective radii are correlated with Sersic indices (e.g. Young and Currie 2001), in the sense that galaxies with a larger size tend to have a surface brightness profile more peaked in the center. By looking at Fig. 5, we see that, taking into account the dispersion of the KR, the completeness magnitude line begins to intercept the $\log r_e$–$<\mu>_e$ relation at $\log R_e \sim 0.3$, implying that galaxies in the shaded area of Fig 7a start to be lost from

[3] The present data do not allow, in fact, the waveband dependence of the Photometric Plane to be investigated.

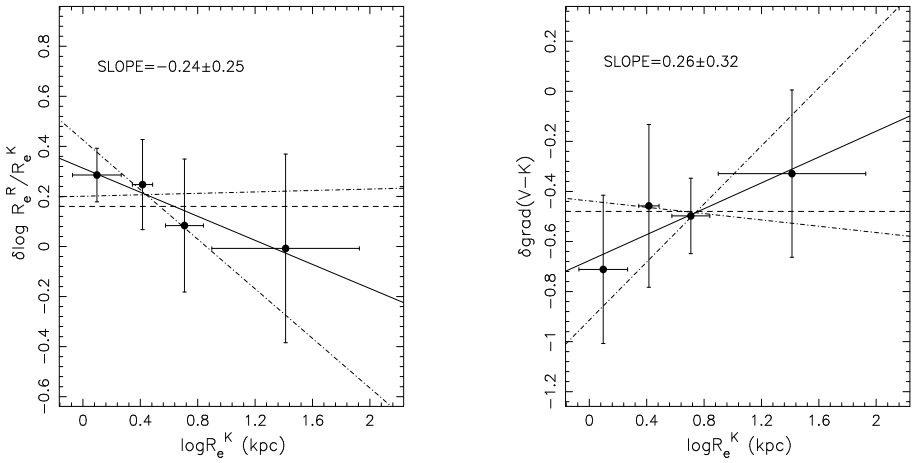


**Fig. 6.** Ratios of optical to NIR effective radii and colour gradients are plotted versus the logarithm of the K-band effective radius. The dashed lines mark the mean values of $\log R_e^R/R_e^K$ and grad(V – K) in the left and right panels, respectively. Data were binned in order to have the same number of points in each bin. The solid lines mark the best-fits to the data, while the dot–dashed lines indicate the $1\sigma$ confidence intervals.

the present sample because of the magnitude selection. We applied a bi-weight least square fit to the data with $\log R_e > 0.3$, minimizing the rms of the residuals with respect to $\log n$. The fit gives $\log n = (0.31 \pm 0.05) \cdot \log R_e + (0.56 \pm 0.1)$, with an rms that amounts to $\sim 0.15$dex ($\sim 35\%$) in n and $\sim 0.5$dex in $\log r_e$, which is much larger with respect to that obtained for the KR ($\sim 0.22 \pm 0.04$ dex). We note that the $\log n$ regression is quite insensitive to selection cuts with respect to $\log r_e$, and, in fact, the above coefficients do not vary significantly including all the galaxies in the fit.

The other panels of Fig. 7 show different projections of the so-called Photometric Plane (PHP). For comparison with GRA02, we adopted the following representation of the PHP:

$$\log R_e = a \cdot \log n + b <\mu>_e + c, \quad (5)$$

which is analogous to the usual equation of the Fundamental Plane (FP), once the velocity dispersion term is replaced with $\log n$. Following GRA02, the coefficients a and b were obtained by a least square fit minimizing the rms of the residuals to $\log R_e$. We also took into account the correlation of the uncertainties on the structural parameters by using the MIST algorithm (La Barbera, Busarello, and Capaccioli, 2000). The fitting results are $a = 0.6 \pm 0.13$, $b = 0.235 \pm 0.02$ and $c = -4.5 \pm 0.25$, with a residual rms of $\sim 0.15$ dex in $R_e$. In order to correct these values for the magnitude cut, we generalized to the 3D case the procedure adopted in the previous section for the KR fit (see LBM03b for details). We found that the bias in the b coefficient is negligible, while it amounts to +30% and −4% for the coefficients a and c, respectively, and to +13% for the dispersion in the $\log R_e$ variable. After correction, the fitting coefficients become $a = 0.8 \pm 0.2$, $b = 0.235 \pm 0.02$ and $c = -4.70 \pm 0.026$, with a corrected $\log r_e$ scatter of $\sim 0.17$ dex, which is smaller by $\sim 14\%$ than that of the KR. The 'corrected' values of a, b and c

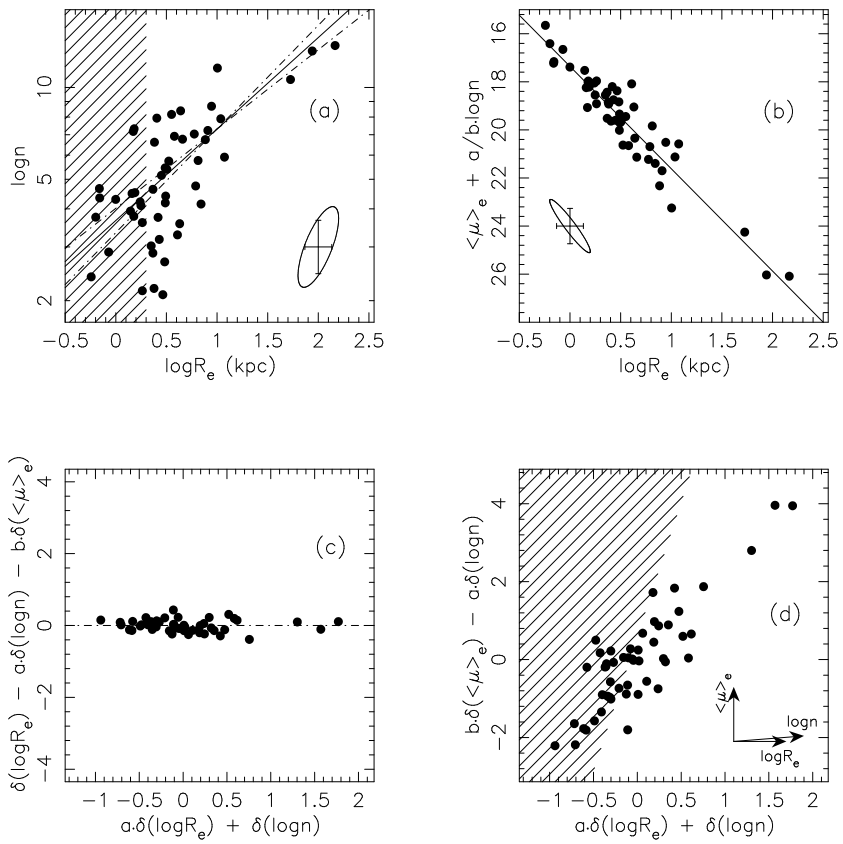


**Fig. 7.** Distribution of galaxies in the space of structural parameters. Upper–left: $\log R_e$–$\log n$ relation. The ellipses in the upper plots are the 68% probability contours. The solid and dot–dashed lines are the best–fit and the $1\sigma$ confidence lines, respectively. The region affected by the magnitude selection is filled by a dashed pattern. Upper–right: edge-on projection of the PHP with the best-fit relation marked by a solid line. Lower–left: 'long' edge-on projection of the PHP. Lower–right: face–on view of the PHP. The shaded region is delimited on the right by the line that results from the intersection of the plane $K_T$ = cost with a plane parallel to the PHP but with zeropoint $c + 2 \cdot \sigma_c$.

were used to obtain the edge-on sections (Fig. 7b, c) and the face-on projection (Fig. 7d) of the PHP.

The slopes and the scatter of the NIR PHP at $z \sim 0.2$ turn out to be in remarkable agreement with those derived by GRA02 for galaxies in the Fornax and Virgo clusters: $a = 0.86 \pm 0.13$, $b = 0.228 \pm 0.036$ and $\sigma_{\log R_e} \sim 0.17$ dex. We point out that the magnitude selection significantly affects the $\log n$ coefficient and that, therefore, it would be very interesting to use a sample of galaxies spanning a larger magnitude range in order to better constrain this coefficient. The selection effects can be further illustrated by looking at the face-on projection of the PHP in Fig. 7d. Due to the finite dispersion of the galaxies around the PHP, its intersection with the plane $K_T$ = cost results in a 'strip'. As a consequence, the distribution of the galaxies in the shaded area of the figure is not 'complete'. On the other hand, the lack of galaxies in the right region of Fig. 7d is real, and corresponds to the well-known 'avoidance' region, which has been

discussed in FP studies (e.g. Jørgensen, Franx, and Kjærgaard 1996).

In order to estimate the intrinsic dispersions of the $\log R_e$–$\log n$ relation and of the PHP, we subtracted to the observed dispersion in $\log R_e$ the amount of scatter expected from the measurement errors on the observed parameters, taking into account the covariance terms between the uncertainties on $\log R_e$, $<\mu>_e$ and $\log n$. The intrinsic dispersions of the $\log R_e$–$\log n$ relation and of the PHP turn out to be $\sim 0.45$ dex and $\sim 0.16$ dex, respectively. Interestingly, the measurement errors account only for few percents of the observed dispersion around the PHP, because, as shown in Fig. 7b, their correlation is almost parallel to the plane, in the same way as for the KR.

## 7. Discussion and Conclusions

In the second of two papers, we have studied the structural properties of the galaxies in the cluster A 2163B at $z \sim 0.2$. Surface photometry has been derived in the R, I and K bands for $N \sim 60$ galaxies, and has been used to

i) compare galaxy structural parameters at optical and NIR wavelengths, and to estimate the optical and NIR internal colour gradients;
ii) perform for the first time a comparative optical/NIR analysis of the KR;
iii) derive the PHP of spheroids at $z \sim 0.2$ in the K band.

The characteristics of the light distribution in galaxies (effective radius, mean surface brightness and Sersic index) are the same between the optical wavebands, while a significant difference is found when comparing optical to NIR parameters. Effective radii decrease by $40 \pm 10\%$ from the R to the K bands, implying that the light profile in galaxies is much more concentrated in the NIR than in the optical. On the other hand, surface brightnesses show a waveband dependence that is fully explained by the behaviour of $r_e$ and by the $R-K$ galaxy colours. For what concerns Sersic indices, they seem to be slightly higher in the K band, implying a stronger curvature of the NIR light profile. The value of $r_e^{OPT}/r_e^{NIR}$ is consistent with what we found in previous works on the optical/NIR structural parameters of cluster galaxies at $z \sim 0.3$ and at $z \sim 0.6$ (see LBM02 and LBM03a), and with the findings of Nelson et al. (2002) for the WFPC2/NICMOS effective radii of brightest cluster galaxies at $0.4 < z < 0.8$ ($r_e^{NIR}/r_e^{OPT} \sim 0.5$). The ratio of optical to NIR radii is also consistent with that found for nearby early-types by Rembold et al. (2002) $r_e^{NIR}/r_e^{OPT} \sim 0.5$, and is in agreement, although slightly larger (by $\sim 2\sigma$), with that found by Pahre, de Carvalho, and Djorgovski (1998), $r_e^{OPT}/r_e^{NIR} \sim 1.2$.

The population of spheroids in A 2163B has null colour gradients at optical wavelengths ($V-R$ restframe) and $V-K$ restframe gradients that, on average, amount to $-0.48 \pm 0.06$ mag/dex. As shown by LBM03a, this value does not evolve significantly over redshift, and, together with UV-optical colour gradient measurements, implies that spheroids have a metallicity gradient of about $-0.2$dex per decade of radius, which is consistent with other studies of colour gradients for both nearby and intermediate redshift galaxies (Saglia et al. 2000; Idiart et al. 2002). We note

that the dissipative monolithic collapse model for the formation of early-type galaxies predicts a chemical abundance gradient of about $-0.5$ (Carlberg, 1984), which is not consistent with the above results. On the other hand, merging mixes the SPs between the inner and outer galaxy regions (White, 1980), and therefore shallower chemical gradients can be well understood within the hierarchical merging framework.

We have studied for the first time the variation of structural parameters as well as of colour gradients along the galaxy sequence by deriving the KR both at optical and NIR wavelengths. The slope and the zeropoint of the optical KR are consistent with those obtained in LBM03b. For what concerns the NIR KR, we compare its slope and zeropoint with the optical values by taking into account (i) the colour magnitude relation and (ii) the value of the mean ratio of optical/NIR effective radii. These factors fully explain the difference between the optical and NIR zeropoints. The most interesting result, however, is that the slope of the R-band KR, corrected for the effects (i) and (ii), is lower by $\sim 2.3\sigma$ than the K-band value. This difference can be explained by the fact that the ratio of optical to NIR effective radii (the optical/NIR colour gradient) *decreases (increases)* with galaxy size. A direct inspection of the $\log R_e^R/R_e^K$ and the grad$(V-K)$ vs. $\log R_e^K$ diagrams shows that such trend could be real. In any case, our data can exclude a decrease of colour gradients with galaxy size, which is a natural expectation of the monolithic collapse model: less massive systems have a shallower potential well, and, therefore, the difference in the time scale of the galactic wind injection between the inner and outer regions is shorter for galaxies of smaller sizes. A decrease of colour gradients with galaxy luminosity has been unfruitfully looked for by various studies (e.g. Peletier et al. 1990), while only a possible indication has been found for the population of E + A galaxies at intermediate redshift (Bartholomew et al., 2001). On the other hand, an increase of the ratio between optical and NIR effective radii with galaxy colour (and therefore with luminosity) has been clearly detected by Pierini (2002) for nearby dwarf early-types. In hierarchical merging models, more massive galaxies form from larger disk systems with a stronger colour gradient. Merging is expected to destroy colour gradients (White, 1980), and, therefore, if galaxies with larger size along the $\log r_e - <\mu>_e$ relation have experienced a higher merging rate (Capaccioli, Caon, and D'Onofrio, 1992), their colour profile could be well comparable, or less steep, with respect to that of smaller systems. The data of A 2163B favor this scenario.

Finally, we have analyzed the so-called Photometric Plane (PHP) of the spheroidal population at $z \sim 0.2$. We find that spheroids follow a bivariate relation between K-band effective parameters and the logarithm of the Sersic index: $\log R_e^K \propto a \cdot \log n^K + b \cdot <\mu>_e^K$. Attempting to correct for the correlations among the uncertainties on structural parameters as well as for the selection effects, we find: $a = 0.8 \pm 0.2$ and $0.235 \pm 0.02$, and an observed dispersion of $\sim 0.17$ dex. These values are consistent with the PHP coefficients found by GRA02 in the optical for nearby early-types in the Fornax and Coma clusters. Interestingly, we find that the correlation of the uncertainties on the structural parameters is almost parallel to the PHP, analogously to what happens for the KR. This implies that the intrinsic scatter of the PHP amounts to about 0.16 dex, which is only

few percents smaller than the observed scatter, but ∼ 13% lower with respect to that of the KR (∼ 0.21 dex). Therefore, although the observed scatter around the plane seems to be similar to that of the Fundamental Plane, as found by GRA02, the present data indicate that its intrinsic dispersion could be significantly larger. In a forthcoming paper, we will analyze the previous items by using a large and deeper sample of galaxies at intermediate redshifts.

*Acknowledgements.* We are grateful to M. Pannella, who made part of the observations of A 2163B.

## References

Bartholomew, L.J., Rose, J.A., Gaba, A.E., & Caldwell, N. 2001, AJ, 122, 2913

Barger, A.J., Aragón-Salamanca, A., Smail, I., et al. 1998, ApJ, 501, 522

Bruzual, G.A., & Charlot, S., 1993, ApJ, 405, 538

Caon, N., Capaccioli, M., & D'Onofrio, M., 1993, MNRAS, 265, 1013

Capaccioli, M., Caon, N., & D'Onofrio, M. 1992, MNRAS, 259, 323

Carlberg, R.G. 1984, ApJ, 286, 403

Graham, A. 2002, MNRAS, 334, 859 (GRA02)

Graham, A., & Guzmàn, R. 2003, AJ, in press (astro-ph/0303391)

Idiart, T.P., Michard, R., & de Freitas Pacheco, J.A. 2002, A&A, 383, 30

Jørgensen, I., Franx, M., & Kjærgaard, P. 1995, MNRAS, 273, 1097

Jørgensen, I., Franx, M., & Kjærgaard, P. 1996, MNRAS, 280, 167

Kauffmann, G. 1996, MNRAS, 281, 475

La Barbera, F., Busarello, G., & Capaccioli, M. 2000, A&A, 362, 851

La Barbera, F., Busarello, G., Merluzzi, P., Massarotti, M., & Capaccioli, M. 2002, ApJ, 571, 790 (LBM02)

La Barbera, F., Busarello, G., Massarotti, M., Merluzzi, P., & Mercurio, A. 2003a, A&A, in press (astro-ph/0211478) (LBM03a)

La Barbera, F., Busarello, G., Massarotti, M., Merluzzi, P., & Capaccioli, M. 2003b, ApJ, in press (astro-ph/0212294) (LBM03b)

La Barbera, F., Massarotti, M., Merluzzi, P., Busarello, G., & Mercurio, A. 2003c, A&A, submitted (paper I)

Larson, R.B. 1974, MNRAS, 166, 585

Lima Neto, G.B., Gerbal, D., & Márquez, I. 1999, MNRAS, 309, 481

Lubin, L.M., & Sandage, A. 2001, AJ, 122, 1084

Márquez, I., Lima Neto G.B., Capelato, H., et al. 2000, A&A, 353, 873

Nelson, A.E., Simard, L., Zaritsky, D., Dalcanton, J.J., & Gonzalez, A.H. 2002, ApJ, 567, 144

Pahre, M.A., Djorgovski, S.G., & de Carvalho, R.R. 1996, ApJ, 456, 79

Pahre, A.M., de Carvalho, R.R., & Djorgovski, S.G. 1998, AJ, 116, 1606

Peletier, R.F., Davies, R.L., Illingworth, G.D., Davis, L.E., & Cawson, M. 1990, AJ, 100, 1091

Peletier, R.F., Valentijn, E.A., & Jameson, R.F. 1990, A&A, 233, 62

Pierini, D. 2002, MNRAS, 330, 997

Rembold, S.B., Pastorizia, M.G., Dicati, J.R., Rubio, M., & Roth, M. 2002, A&A, 391, 531

Saglia, R.P., Maraston, C., Greggio, L., Bender, R., & Ziegler, B. 2000, A&A, 360, 911

Sandage, A., & Perelmuter, J.-M. 1991, ApJ, 370, 455

Sandage, A., & Lubin, L.M. 2001, AJ, 121, 2271

Tamura, N., & Ohta, K. 2000, AJ, 120, 533

Young, C.K., & Currie, M.J. 2001, A&A, 369, 736

White, S.D. 1980, MNRAS, 191, 1

Ziegler, B.L., Saglia, R.B., Bender, R., et al. 1999, A&A, 346, 13